Received 8 August 2025; Accepted 8 September 2025
https://doi.org/10.48612/letters/2025-4-230-235
https://elibrary.ru/babxvr

Effect of surface magnetism on ferromagnetic films with an antidote lattice: Monte Carlo simulation

S. V. Belim†, S. S. Simakova

†sbelim@mail.ru

Omsk State Technical University, Omsk 644050, Russia

Abstract: This article presents a Monte Carlo simulation of thin ferromagnetic films with an antidote lattice in an external magnetic field. The simulation studies films with an easy magnetization axis described by the Ising model. The Metropolis algorithm and finite-dimensional scaling theory are used to simulate the film behavior. The antidote lattice is an ordered array of square pores. The pores are located at the nodes of a regular square grid. The lattice period remains constant in the calculations, while the pore sizes vary. The calculations result in hysteresis loops for films with different thicknesses and pore sizes of the antidote lattice at different ratios of exchange constants. The calculations show that surface magnetism can have a different effect on the dependence of the coercive force on the pore size. At ratios of exchange constant close to unity, the antidote lattice reduces the coercive force and magnetization energy. At large relative values of the surface exchange constant, the antidote lattice increases the coercive force in the film. Calculations show the existence of conditions under which the antidote lattice does not affect the film magnetization. The article considers the case of large pore sizes. A sharp increase in coercive force is observed in this case. If the pore size exceeds 90% of the antidote lattice period, then a sharp decrease in coercive force occurs. The simulation results are in good agreement with the experimental data.

Keywords: coercive force, antidote lattice, ferromagnetic thin films, surface magnetism, Monte Carlo simulation

1. Introduction

Ferromagnetic films acquire new properties when an array of nanopores is formed in them [1]. The pores are located at the nodes of a regular grid and form an antidote lattice. The pores increase the free surface of the film, which affects its magnetic properties [2]. The main advantage of such materials is the ability to control magnetic properties by changing the geometric parameters. Due to this capability, films with an antidote lattice are widely used in spintronic devices, where materials with predetermined magnetic characteristics are required. Coercive force and remagnetization energy are among such parameters. These two parameters affect the power consumption of spin valves and other spintronic devices. Predicting the pore size and the antidote lattice period is an important problem in the manufacture of such devices. Films with uniaxial magnetic anisotropy are the most commonly used in spintronics. These films have reduced power consumption and increase the efficiency of random-access memory [3 – 5]. Both single-layer and double-layer films are used in spintronic devices [6, 7].

The main effect of the antidote lattice is to increase the free surface of the film. An increase in the area of the free border increases the influence of surface phenomena. One of these phenomena is surface magnetism, which affects magnetization in thin films. The phenomenon of surface magnetism increases the total magnetic energy of the system [8, 9]. Surface magnetism occurs in materials for which the intensity of the exchange interaction between surface spins exceeds the bulk value [10,11]. This difference is observed in several materials widely used in technological processes, such as Fe, Co and Mn [12]. In addition to increasing the free surface area of the thin film, the antidote lattice creates the interaction of its two free boundaries. Surface magnetism changes the Curie temperature and the coercive force of the system in continuous films [13].

Experimental studies of magnetization in ferromagnetic films with an antidote lattice show opposite results for different materials. The hysteresis loop can either expand or decrease with the addition of an ordered pore array. In the first case, the coercive force and the magnetization energy increase. In the second case, both parameters are reduced. For example, the coercive force increases with increasing pore diameter in Co (0.5 nm)/Pd (0.5 nm) multilayer structures [14 –16]. The coercive force decreases with the addition of the antidote lattice in Co (0.5 nm)/Pt (1 nm) multilayer structures [17]. GdFe films with an antithesis lattice with a period of 200 nm are studied in [18]. These films have strong magnetic anisotropy along the axis perpendicular to the plane of the film. Hysteresis loops were obtained experimentally for two pore sizes (95 nm and 120 nm). The width of the hysteresis loop decreases with increasing pore size, which reduces the coercive force. The process of magnetization in a multilayer film Ta (5 nm)/Pt (5 nm)/Co (0.6 nm)/FeMn (X)/Ta (5 nm), (X = 0, 2, 3.5, 5.5 nm) was investigated in [19] for an antidote lattice with a period of 100 nm and 150 nm and a pore diameter of 40 nm and 55 nm. The coercive force in these

films can either increase or decrease with increasing pore diameter depending on the thickness of the FeMn layer. Micromagnetic modeling of Fe films with an antidote lattice was performed in [20] considering the dipole-dipole interaction. In the simulation, the pore sizes were constant, the period of the antidote lattice changed. The calculations made in this work show a decrease in coercive force with an increase in the distance between the pores. This conclusion is consistent with the experimental results for Fe. Similar results were obtained experimentally for Ni and FeNi films [21].

Some surface effects were studied experimentally in [22] for Co/Pd films with a thickness of 12 nm and an antidote lattice with a period of 202 nm. Pore sizes range from 128 nm to 182 nm. Experimental measurements showed first a nonlinear increase in the coercive force, and then a sharp decrease with increasing pore size. Micromagnetic modeling was carried out in the same work, considering defects and changes in the anisotropy parameter in a thin near-surface layer. Varying the surface anisotropy parameter demonstrates different results in the coercive force behavior with increasing pore size. The coercive force increases with increasing pore diameter at high anisotropy values and decreases at low values. However, the results of micromagnetic modeling do not completely coincide with the experimental curve. The coercive force growth is less rapid, and there is no area with a decrease in the coercive force. More complete agreement with the experiment is observed when accounting for surface defects.

Monte Carlo simulation of thin films with an antidote lattice without considering surface effects [23] showed a decrease in the coercive force and magnetization energy. The surface magnetism phenomena in continuous films [24] can change the phase diagram of the system and affect the process of their magnetization. The aim of this article is to study the effect of surface magnetism on the process of magnetization of thin ferromagnetic films with an antidote lattice using

2. Model

The simulated system is a film of $L\times L$ atoms and thickness D of monoatomic layers (ML). The film is parallel to the OXY coordinate plane. The free film boundaries have the equations $z=0$ and $z=D-1$. To simulate infinite films, periodic boundary conditions are specified in the system along the OX and OY axes. The antidote lattice is an array of square pores of size $a\times a$ and period d. The geometric parameters of the system are shown in Fig. 1.

The simulated films have an easy magnetization axis. This anisotropy is experimentally observed in thin ferromagnetic films with an antidote lattice [3 – 5]. The direction of the easy axis does not affect the simulation results if the direction of the external magnetic field coincides with the direction of this axis. The Ising model is applicable to simulate the magnetic properties of films with such anisotropy. In this model, each atom (i,j) has a spin S_{ij} that can take two values (+1/2 or −1/2). The interaction between spins is exchangeable in this model. The exchange interaction is short-range, so the calculations only consider the energy for the pairs of nearest neighbors. In this case, the energy of the exchange interaction is determined by a certain constant. Exchange forces have

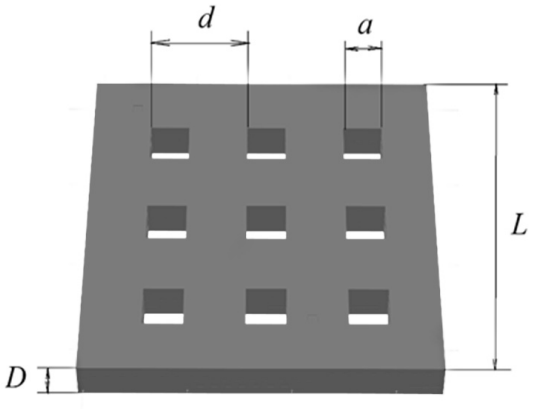

Fig. 1. Geometric parameters of the model.

constant J in the bulk. Exchange forces on the surface may differ from bulk forces [6,7,12] and have the exchange constant $J_S(J_S \geq J)$. The difference in exchange constants on the surface and in the bulk is a consequence of the distortion of the crystal lattice and the electronic structure near the free boundary. These distortions can be the cause of surface magnetism. The Hamiltonian of the system is equal to the sum of the interaction energies for the nearest neighbors.

$$H_0 = -J\sum_{\text{Bulk}} S_{ij}S_{kl} - J_S \sum_{\text{Surface}} S_{ij}S_{kl} - J_{BS}\sum_{\text{S/B}} S_{ij}S_{kl} - \mu_B h_0 \sum S_{ij}. \quad (1)$$

The Hamiltonian includes four terms. The first term is equal to the energy of the spins in the bulk with the exchange constant J. The second term is equal to the energy of the exchange interaction for pairs of surface spins with the exchange constant J_S. The third term determines the interaction for the surface layer of spins with the first subsurface layer with the constant J_{BS}. The exchange constant JBS is calculated based on the combining rule $J_{BS}=(J\cdot J_S)^{1/2}$ [25]. Surface magnetic phenomena decrease inside the film according to the exponential law, so the constants differ only in the monoatomic surface layer during modeling. The fourth term is equal to the interaction energy of the spins in the film with an external magnetic field with a strength h_0. μ_B is the Bohr magneton.

Relative units are more convenient for computer simulation: $R=J_S/J$, $h=\mu_B h_0/J$. The Hamiltonian in these units is:

$$H = H_0 / J = -\sum_{\text{Bulk}} S_{ij}S_{kl} - R\sum_{\text{Surface}} S_{ij}S_{kl} - \sqrt{R}\sum_{\text{S/B}} S_{ij}S_{kl} - h\sum S_{ij}. \quad (2)$$

Relative units are also used for system temperature T: $T=k_B t/J$. k_B is the Boltzmann constant. t is the thermodynamic temperature.

The magnetization in the system m in relative units is equal to the average spin value per unit volume.

$$m = \left(\sum_{i,j=1}^{L} S_{ij}\right) \Big/ N. \quad (3)$$

N is the number of spins per unit volume.

The finite-dimensional scaling theory is used in modeling infinite systems based on finite its [26]. Spin configurations are formed using the Metropolis algorithm [27]. Spin averaging is used to obtain the values of thermodynamic functions.

The magnetization process is studied in the ferromagnetic phase to produce hysteresis loops. Therefore, the Curie temperature of the system is calculated in the first simulation step. The phase transition temperature is determined based on the fourth order energy cumulants for bulk V and surface V_S of film.

$$V = 1 - \frac{\langle E^4 \rangle}{3\langle E^2 \rangle^2}, V_S = 1 - \frac{\langle E_S^4 \rangle}{3\langle E_S^2 \rangle^2}. \quad (4)$$

E is the interaction energy between the spins within the system. E_S is the interaction energy between surface spins. Angle brackets denote averaging over spin configurations.

Dependence of fourth-order energy cumulant on temperature has minimum at the phase transition point. It should be noted that the method for determining the Curie point from the energy cumulant is not very accurate. More accurate values can be obtained based on Binder cumulants [26]. However, this method has higher computational complexity. However, the accuracy of the energy cumulant method is sufficient to study hysteresis phenomena. The magnetization in the system is studied in the ferromagnetic phase significantly below the Curie point.

To calculate the hysteresis loop, the system is initially placed in a strong magnetic field h_m. This field orients all the spins in the same direction. After that, the field decreases in increments Δh to the value $-h_m$. Then the field is increased again in increments Δh to the value h_m. Transitioning to a new state requires ΔN Monte Carlo steps per spin. The magnetization m is calculated for each magnetic field strength. The plot of magnetization m versus magnetic field h shows a hysteresis loop. The intersection of the hysteresis loop with the abscissa axis H_{C1} and H_{C2} determines the coercive force $H_C = (H_{C1} + H_{C2})/2$. The hysteresis loop area determines the magnetization energy of the film E_m in relative units.

3. Results

The magnetization process is modeled for films with different thicknesses and linear dimensions equal to $L = 64$. The film thickness varies from $D = 4$ ML to $D = 16$ ML in increments $\Delta D = 2$ ML. Simulations are performed for both continuous and antidote lattice films. The antidote lattice period is $d = 8$. The square pore sizes are $a = 2$, $a = 4$ and $a = 6$. The ratio of exchange constants varies from $R = 1.0$ to $R = 2.5$ with step $\Delta R = 1.0$. The ratio of exchange constants usually does not exceed 2.0 for real materials. The ratio of exchange constants depends on the film substance and the crystallographic direction of the free surface: $R(\text{Fe}(110)) = 1.219$, $R(\text{Fe}(001)) = 1.365$, $R(\text{Co}(001)) = 1.535$ [12]. The maximum value of the magnetic field is $h_m = 1.0$. Magnetic field intensity variation step equals $\Delta h = 0.01$. To establish the initial equilibrium, 10^5 Monte Carlo steps per spin are performed. When moving to a new magnetic field strength value, $\Delta N = 100$ Monte Carlo steps per spin are performed.

Critical temperature calculations are performed for systems with linear sizes from $L = 32$ to $L = 64$ with a step of $\Delta L = 8$. The dependence of cumulant V on temperature is plotted with a step of $\Delta T = 0.01$. This step determines the accuracy for the Curie temperature calculation. Simulations show an increase in the critical temperature for all films with increasing exchange constants ratio and film thickness. The minimum Curie temperature is $T_C = 3.81$ for films with thickness $D = 4$ ML. Magnetization is simulated at $T = 2.5$. This temperature provides a ferromagnetic phase for films of any thickness with pores of all sizes.

Continuous films are studied in the first step. Calculations show an increase in the width of the hysteresis loop with an increase in the ratio of exchange constants for films with any thickness. Examples of hysteresis loops for a continuous film with thickness $D = 8$ ML at different ratios of exchange constants R are shown in Fig. 2.

The growth of the surface exchange constant increases the width of the hysteresis loop and increases the coercive force H_C. This dependence is due to a more intense exchange interaction between surface spins, which prevents the direction of magnetization for the entire film from changing. The influence of surface magnetism decreases with increasing film thickness and the width of the hysteresis loop changes less. The dependence of coercive force on the ratio of exchange constants R for films with thickness $D = 16$ and different size is shown in Fig. 3.

The plots in Fig. 3 demonstrate that the effect of the antidote lattice on the coercive force H_C depends on the exchange constants ratio R. If the exchange constant on the surface is equal to the constant in the system bulk, then the

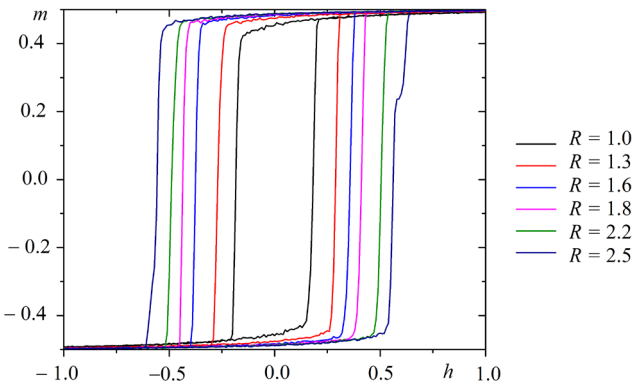

Fig. 2. (Color online) Hysteresis loops for continuous films with thickness $D = 8$ ML for different ratio of exchange constants R.

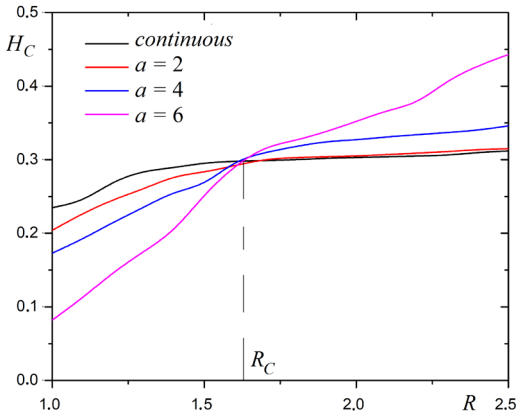

Fig. 3. (Color online) Coercive force plots H_C versus the ratio of exchange constants R for films with a thickness $D = 16$ ML and an antidote lattice with pores with different sizes a.

addition of the antidote lattice reduces the coercivity of the film. However, increasing the surface exchange constant increases the coercive force for the film. Moreover, its growth rate increases with increasing pore sizes. The addition of an antidote lattice increases coercive force at a high value of the exchange constants ratio. Figure 3 also shows that there is a critical value R_C at which the plots for the dependence of coercive force on the exchange constants ratio intersect. The coercive force for the film does not depend on the size of the pores in the antidote lattice under the condition $R=R_C$. Plots for coercive force H_C versus the exchange constants ratio R are similar for all film thickness. The value R_C changes as the film thickness increases. A plot for R_C versus film thickness D is shown in Fig. 4.

The plot in Fig. 4 shows the decrease in the critical value R_C with increasing film thickness D. Moreover, the rate of decrease R_C decreases with increasing film thickness D.

A similar relationship is observed for the magnetization energy. Plots for the dependence of the magnetization energy E_m on the exchange constants ratio R at different pore sizes a and film thickness D=16 are presented in Fig. 5.

As can be seen from Fig. 5, the magnetization energy shows the same patterns as the coercive force. Plots intersect at the same critical value R_C. The laws for coercive force and magnetization energy coincide, since the shape of the hysteresis loop remains unchanged, only its width changes.

Experimental studies generally examine the change in coercive force with increasing pore size for a particular material. In this case, the exchange constants ratio R remains the same. The dependence of the coercive force H_C on the pore size a at several exchange constants ratio R for a film with a thickness D=16 ML is shown in Fig. 6.

As Fig. 6 shows, the coercive force can both increase and decrease with increasing pore sizes. The determining factor is the surface exchange constant. Its magnitude determines the influence of the free surface.

A previous computer experiment was performed on an antidote lattice with $a \le 0.75d$. Experimental studies also study systems with pore size $a > 0.75d$ [22]. Modeling of this case is carried out in a computer experiment with an antidote lattice period $d=50$ for films with a thickness $D=20$ ML. The pore size varies from $a=5$ to $a=49$. The calculation results are shown in Fig. 7.

Figure 7 shows the change in the coercive force plot behavior at large pore sizes ($d>0.75$). At low values, the shape of the plot is close to linear. After the threshold value $a=0.75d$, a sharp increase in the coercive force is first observed, and then its sharp decrease. The maximum coercive force value corresponds to the pore size $a=0.9d$. A change in the nature

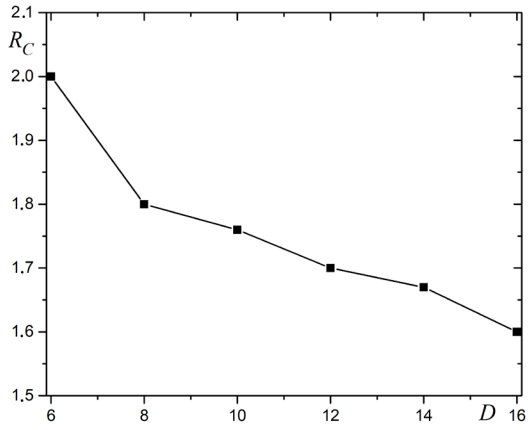

Fig. 4. (Color online) Plot for critical R_C vs. film thickness D.

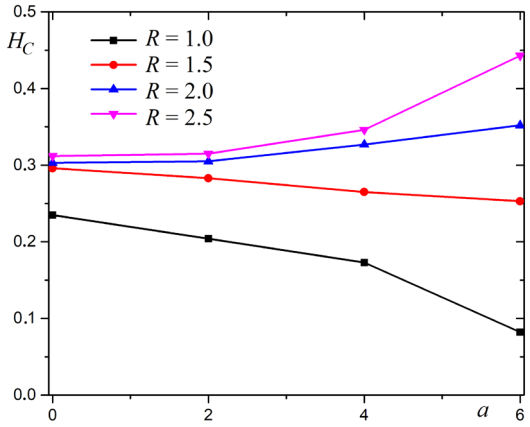

Fig. 6. (Color online) The dependence of the coercive force H_C on the pore size a at several exchange constants ratio R for a film with a thickness D=16 ML.

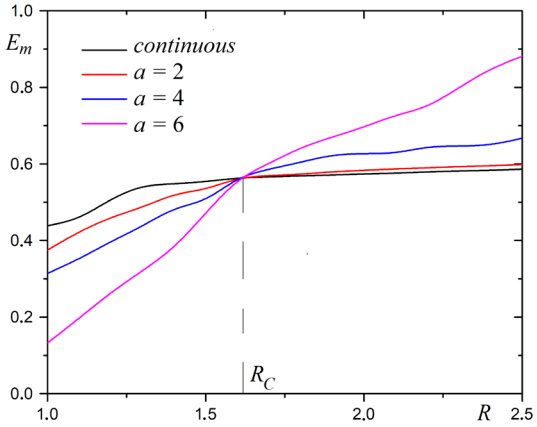

Fig. 5. (Color online) Plots for the dependence of the magnetization energy E_m on the exchange constants ratio R at different pore sizes a and film thickness D=16 ML.

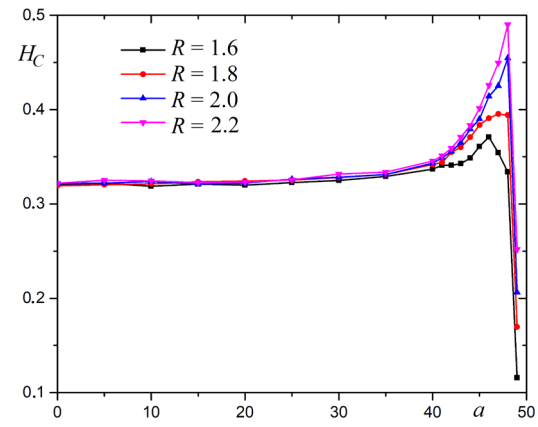

Fig. 7. (Color online) Plots for coercive force H_C vs. pore size a for film thickness D=20 ML and antidote lattice period d=50. R is the exchange constants ratio.

of coercive force behavior is a consequence of a change in the structure of the system. If the pore size is $a \geq 0.9d$, then the system should not be considered as a film, but as a set of intertwined nanowires.

4. Discussion

Let us compare the results obtained with experimental data. The article [22] presents a coercive force versus pore diameter curve for a Co/Pd film with a thickness 12 nm and a lattice period 202 nm. This curve shows an increase in coercive force at a pore diameter from 0 nm (continuous film) to 190 nm, followed by a sharp decrease. The results of the computer modeling carried out are in good agreement with this article. The coercive force versus pore size plot is the same as the curve obtained from the experimental points [22].

The accuracy of the simulation results is also confirmed by experimental measurements for Fe films with an antidote lattice [18]. Studies were performed for films with a thickness 20 nm and an antidote lattice with a period 200 nm. The pore sizes in this work vary from 45 nm to 175 nm. In the coercive force versus pore size plot, linear growth is observed at a pore diameter less than 150 nm with a further sharp jump. The authors of the article did not consider large pores, so there is no decline in coercive force on the plot.

Coercive force measurements in [19] for Ta(5 nm)/Pt (5 nm)/Co(0.6 nm)/FeMn(X)/Ta(5 nm), (X = 0, 2, 3.5, 5.5 nm) showed that an increase in film thickness leads to an increase in coercive force, which is in good agreement with the results obtained in this article. In addition, in the absence of an FeMn layer in the composite film, the addition of an antidote lattice increases the coercive force. This result is consistent with other work that has investigated cobalt-based films. However, when an FeMn layer is added, the antidote lattice reduces coercive force. This implies a decrease in the surface magnetic energy of the system. As shown in [12], based ab initio calculations, the ratio of exchange constants for iron is lower than for cobalt.

The greatest effect of the antidote lattice on the coercive force is observed in the multilayer CoO/Co film [28]. The pore array increases coercive force by a factor 27. Such a great significance cannot be explained by surface magnetism alone. The authors of this work suggest an explanation based on the formation of anti-vortex structures around pores. However, this mechanism also does not produce such a large increase in coercivity. The combined effect of these two factors explains the result.

5. Conclusion

Surface magnetism affects the magnetization process in thin ferromagnetic films with an antidote lattice. This influence results from an increase in the total energy of the exchange interaction between the spins in the material. An increase in the exchange integral on the surface causes an increase in the coercive force. The magnetization energy is also increased. The antidote lattice in a thin film can both lower and increase its coercive force. The effect of the antidote lattice depends on the pore size and surface magnetic energy. The addition of an antidote lattice in the thin film increases the free surface area and increases the number of spins on the surface. This factor has two multidirectional influences. First, surface spins have fewer neighbors, which reduces their exchange interaction energy. As a result, the coercive force for the film is reduced. Secondly, the exchange integral on the surface can exceed the value in the system volume, which increases the energy of the exchange interaction and increases the coercive force. As a result, the coercive force for the film is increased. If the exchange energy at the surface is close in value to the exchange energy in volume, then the first factor dominates. If the surface exchange energy is significantly larger than the value in volume, then the second factor dominates. There is an exchange integral value where both factors balance each other. In this case, the antidote lattice does not affect the coercivity of the film. Film thickness also affects its coercivity. Computer simulations reveal common patterns for changing magnetic characteristics depending on geometric parameters.

References

1. J. He, Z. Zhang, Z. Bao, G. Sun, X. Li, X. Qiu, S. Wang, Z. Wang, Q. Huang, S. Yi, Effect of Ta Interlayers on Texture and Magnetic Properties of FeSi Films with Micrometer Thickness, Materials 15 (2022) 6789.
2. S.K. Abbas, M. Saleem, S. Naseem, S. Riaz, S. Atiq, Synthesis of $Ni_{80}Fe_{20}$ permalloy antidots for high storage ferroelectric memories, Materials Letters 271 (2020) 127852.
3. C. Zhang, W. Li, D. Yu, Y. Wang, M. Yin, H. Wang, Y. Song, X. Zhu, P. Chang, X. Chen, D. Li, Wafer-Scale Highly Ordered Anodic Aluminum Oxide by Soft Nanoimprinting Lithography for Optoelectronics Light Management, Adv. Mater. Interfaces 4 (2017) 1601116.
4. M. Salaheldeen, L. Martínez-Goyeneche, P. Álvarez-Alonso, A. Fernández, Enhancement the perpendicular magnetic anisotropy of nanopatterned hard/soft bilayer magnetic antidot arrays for spintronic application, Nanotechnology 31 (2020) 485708.
5. S. Saha, P.C. Mahato, S. Paul, S.S. Banerjee, Understanding the behavior of exchange bias and coercive fields and connections with anisotropic interfaces in Co_2C nanoparticle system, Phys. Rev. Materials 8 (2024) 116001.
6. A.S. Kamzin, R.G. Glyantsev, Surface and volume phase states of $Fe_{1-x}Ga_xBO_3$ crystals in the vicinity of the Néel point, Phys. Solid State 45 (2003) 2309 – 2312.
7. U. Gradmann, Surface magnetism, Journal of Magnetism and Magnetic Materials 100 (1991) 481 – 496.
8. A. Mitrofanov, G. Chen, A. Kozhanov, S. Urazhdin, Exchange bias without directional anisotropy in permalloy/CoO bilayers, Phys. Rev. B 104 (2021) 144413.
9. M. Campagna, Surface magnetism: Recent progress and opportunities, Journal of Vacuum Science & Technology A: Vacuum, Surfaces, and Films 3 (1985) 1491–1495.
10. M. Potthoff, W. Nolting, Surface magnetism studied within the mean-field approximation of the Hubbard model, Phys. Rev. B 52 (1995) 15341–15354.
11. P.A. Korzhavyi, A.V. Ruban, J. Odqvist, J.-O. Nilsson, B. Johansson, Electronic structure and effective chemical

and magnetic exchange interactions in bcc Fe-Cr alloys, Phys. Rev. B 79 (2009) 054202.
12. I. Turek, S. Blügel, G. Bihlmayer, P. Weinberger, Exchange Interactions at Surfaces of Fe, Co, and Gd, Czechoslovak Journal of Physics 53 (2003) 81–88.
13. M. Pajda, J. Kudrnovský, I. Turek, V. Drchal, P. Bruno, *Ab initio* calculations of exchange interactions, spin-wave stiffness constants, and Curie temperatures of Fe, Co, and Ni, Phys. Rev. B 64 (2001) 174402.
14. T.N. Anh Nguyen, J. Fedotova, J. Kasiuk, W.-B. Wu, J. Przewoźnik, C. Kapusta, O. Kupreeva, S. Lazarouk, T.H. Thuy Trinh, K. Tung Do, H. Manh Do, D. Lam Vu, J. Åkerman, Enhanced Perpendicular Exchange Bias in Co/Pd Antidot Arrays, J. Electron. Mater. 48 (2019) 1492–1497.
15. W.-B. Wu, J. Kasiuk, T.N. A. Nguyen, J. Fedotova, J. Przewoźnik, C. Kapusta, O. Kupreeva, S. Lazarouk, K.T. Do, T.H. Nguyen, H.K. Vu, D.L. Vu, J. Åkerman, Complex magnetic ordering in nanoporous $[Co/Pd]_5$-IrMn multilayers with perpendicular magnetic anisotropy and its impact on magnetization reversal and magnetoresistance, Phys. Chem. Chem. Phys. 22 (2020) 3661–3674.
16. W.-B. Wu, J. Kasiuk, T.N. A. Nguyen, J. Przewoźnik, J. Fedotova, C. Kapusta, O. Kupreeva, S. Lazarouk, K.T. Do, T.H. Nguyen, H.K. Vu, H.L. Pham, D.L. Vu, J. Åkerman, Influence of interfacial magnetic ordering and field-cooling effect on perpendicular exchange bias and magnetoresistance in nanoporous IrMn/[Co/Pd] films, Journal of Applied Physics 127 (2020) 223904.
17. Z. Shi, X.X. Fan, P. He, S.M. Zhou, H.N. Hu, M. Yang, J. Du, Exchange bias of perpendicularly magnetized $[Co/Pt]_3$/IrMn multilayer on porous anodized alumina, Journal of Applied Physics 113 (2013) 17D722.
18. U. Wiedwald, J. Gräfe, K.M. Lebecki, M. Skripnik, F. Haering, G. Schütz, P. Ziemann, E. Goering, U. Nowak, Magnetic switching of nanoscale antidot lattices, Beilstein J. Nanotechnol. 7 (2016) 733–750.
19. F. Fettar, L. Cagnon, D. Barral, P. David, L. Naudin, F. Blondelle, F. Gay, Investigation of magnetic hysteresis in biased Ta/Pt/Co/FeMn/Ta antidots: Influence of structural dimensions, Journal of Applied Physics 135 (2024) 013903.
20. J.M. Torres Bruna, J. Bartolomé, L.M. García Vinuesa, F. Garcia Sanchez, J.M. Gonzalez, O.A. Chubykalo-Fesenko, A micromagnetic study of the hysteretic behavior of antidot Fe films, Journal of Magnetism and Magnetic Materials 290–291 (2005) 149–152.
21. M. Vázquez, K.R. Pirota, D. Navas, A. Asenjo, M. Hernández-Vélez, P. Prieto, J.M. Sanz, Ordered magnetic nanohole and antidot arrays prepared through replication from anodic alumina templates, Journal of Magnetism and Magnetic Materials 320 (2008) 1978–1983.
22. M. Krupinski, P. Sobieszczyk, P. Zieliński, M. Marszałek, Magnetic reversal in perpendicularly magnetized antidot arrays with intrinsic and extrinsic defects, Sci. Rep. 9 (2019) 13276.
23. S.V. Belim, S.S. Simakova, I.V. Tikhomirov, Effect of disorder on phase transitions in antidote lattice thin films: computer simulations, Letters on Materials 13 (2023) 304–307. DOI: 10.22226/2410-3535-2023-4-304-307 Webpage
24. S.V. Belim, E.V. Bogdanova, A study of the surface phase transition in epitaxial antiferromagnetic films by Monte Carlo simulation, Journal of Magnetism and Magnetic Materials 599 (2024) 172107.
25. M. Waldman, A.T. Hagler, New combining rules for rare gas van der waals parameters, J. Comput. Chem. 14 (1993) 1077–1084.
26. K. Binder, Critical Properties from Monte Carlo Coarse Graining and Renormalization, Phys. Rev. Lett. 47 (1981) 693–696.
27. D.P. Landau, K. Binder, Phase diagrams and multicritical behavior of a three-dimensional anisotropic Heisenberg antiferromagnet, Phys. Rev. B 17 (1978) 2328–2342.
28. M. Salaheldeen, A. Nafady, A.M. Abu-Dief, R. Díaz Crespo, M.P. Fernández-García, J.P. Andrés, R. López Antón, J.A. Blanco, P. Álvarez-Alonso, Enhancement of Exchange Bias and Perpendicular Magnetic Anisotropy in CoO/Co Multilayer Thin Films by Tuning the Alumina Template Nanohole Size, Nanomaterials 12 (2022) 2544.